



Research article

Chitosan-Coated Azithromycin-Loaded PLGA Nanoparticles: Characterization and Potential for Enhanced Antibacterial Activity

Bao Ngoc Tran^a, Nhu To Bui^a, Quynh Thi Nhu Nguyen^b, Tiep Khac Nguyen^b, Chien Ngoc Nguyen^{a,c*}

^a Faculty of Pharmaceutics and Pharmaceutical Technology, Hanoi University of Pharmacy, 13-15 Le Thanh Tong, Cua Nam, Hanoi, Vietnam.

^b Faculty of Biotechnology, Hanoi University of Pharmacy, 13-15 Le Thanh Tong, Cua Nam, Hanoi, Vietnam.

^c National Institute of Pharmaceutical Technology, Hanoi University of Pharmacy, 13-15 Le Thanh Tong, Cua Nam, Hanoi, Vietnam.

* Corresponding author: Chien Ngoc Nguyen, email: chiennn@hup.edu.vn

ARTICLE INFO

Article history

Received 13 August 2025

Revised 10 November 2025

Accepted 25 November 2025

Keywords

Azithromycin

PLGA

Chitosan

Nanoparticle

Size distribution

Antibacterial

Staphylococcus aureus.

ABSTRACT

Recent studies have introduced azithromycin (AZT) in multiple formulations that implement nanoparticles (NPs) to enhance its antibacterial efficacy and prevent bacterial resistance. However, the impact of chitosan (CS) coating on AZT-poly(lactic-co-glycolic acid) (PLGA) NPs remains underexplored. This study developed and characterized AZT-PLGA NPs with and without CS coating, focusing on physicochemical properties, *in vitro* release, and antibacterial properties (against *Staphylococcus aureus*). The uncoated and CS-coated NPs exhibited mean particle sizes below 200 nm with narrow polydispersity (PDI < 0.3). CS coating reversed the surface charge from negative to positive values (app. 30 mV), confirming successful deposition. SEM and FTIR analyses indicated a PLGA-rich core with drug-polymer interactions, and a CS layer in coated NPs. *In vitro* release studies revealed that CS-coated NPs showed a more sustained release profile compared to uncoated NPs. Antibacterial evaluation demonstrated that all NP formulations had lower minimum inhibitory concentrations (MIC) than raw AZT, with PLGA-based formulations achieving approximately fourfold MIC reduction. CS-coated NPs showing comparable or slightly lower MBC values than the same formulation without CS. This work presents a new aspect of CS-coated PLGA NPs, offering a potential platform for macrolide antibiotics.

* Correspondence: Chien Ngoc Nguyen, email: chiennn@hup.edu.vn;

<http://doi.org/10.59882/1859-364X/353>

INTRODUCTION

In recent years, the European Medicines Agency (EMA) has raised concerns about the shortage of antibiotics, particularly Azithromycin (AZT), a macrolide substance [1]. In parallel, the increasing prevalence of bacterial resistance to AZT has emerged as a significant therapeutic challenge. The predominant resistance mechanisms include structural modifications of the ribosomal binding site and active efflux of AZT from bacterial cells [2, 3]. To overcome these barriers, nanoparticle-based drug delivery systems can enhance the intracellular delivery of antibiotics, sustain drug release, and improve bioavailability at the site of infection.

In this context, poly(lactic-co-glycolic acid) (PLGA) is a well-established biodegradable polymer approved by the FDA for drug delivery applications [1, 4]. When used as a carrier for AZT, PLGA nanoparticles (NPs) offer an enhanced antibacterial effect. Moreover, surface modification of NPs with cationic polymers such as chitosan (CS) has been shown to enhance mucosal adhesion, cellular uptake, and membrane permeability [2]. In this study, CS coated PLGA NPs may also modulate their physicochemical properties, which are modifying interaction with bacterial membranes.

This study aims to develop and characterize AZT-loaded PLGA nanoparticles (AZT-PLGA NPs) and CS coated AZT-PLGA NPs to provide insight knowledge about polymeric nanocarriers for improving antibiotic performance.

MATERIALS AND METHODS

Materials:

AZT (as azithromycin dihydrate) was obtained from Century pharmaceutical (India). Poly (lactic-co-glycolic) acid PLGA,

50:50 (DLG5050H) was purchased from Lakeshore Biomaterials (Lakeshore Biomaterials, UK). Chitosan (CS), a low molecular weight type, was purchased from Merck SA (Merck KGaA, Darmstadt, Germany). The surfactants are polyvinyl alcohol (PVA, purchased from Xilong, China). All other analytical substances were used at the analytical grade without chemical modification.

Methods:

Preparing AZT loaded PLGA (AZT-PLGA) NPs:

NPs were prepared by the solvent-evaporation method: 30 mg AZT and different weight of PLGA were dissolved in 5 mL acetone. The aqueous phase is 10 mL aqueous solution of PVA (1%). The oil–water mixture was homogenized for 2 min using an ultrasonic processor (UP50H, Hielscher, Germany) with a magnetic stirrer (IKA Lab) at 900 rpm. The obtained nanosuspension was then stirred under vacuum (< 0.1 bar) for 2 h in a 20 L vacuum desiccator (VDR-30) placed on a magnetic stirrer to facilitate continuous agitation and acetone evaporation.

Preparing CS coated AZT-PLGA NPs (CS-AZT-PLGA NPs):

AZT-PLGA NP suspension was stirred with CS 1% solution for 1 h (magnetic stirrer, IKA, Germany). When adding CS, the final suspension was homogenized mechanically by the Benchmark D1000 Homogenizer (5mm generators, Benchmark, USA), set at a frequency of 60 Hz-130W with a rotor speed of 1500 rpm for a duration of 2 min. The CS solution was prepared by mixing 0.1 g CS into 10 mL acetic acid 1% solution. The ratio of CS/PLGA (w/w) were set at 1:2, 1:1, and 2:1 (w/w) in the screening experiments.

Measurement of particle size distribution (Z & PDI) and Zeta potential (ZP):

NPs were analyzed with the average particle size (Z) and polydispersity index (PDI) using the dynamic light scattering (DLS) method. Samples were diluted 20 times with the related aqueous phase before measurements by Zetasizer ZS90 (Marvel Instrument Ltd., Marvel, UK). The measurement conditions were set at $25 \pm 0.1^\circ\text{C}$, with a scattering angle of 173° , and a refractive index of 1.330 for AZT. Measurements were performed with the attenuator adjusted to maintain a count rate of 200-400 kcounts/s.

The ZP was measured with Folded Capillary Zeta Cell cuvettes. Samples were also diluted 20 times before measurements (triplicate each sample).

AZT assay and encapsulation efficiency:

AZT was quantified by HPLC method, referred to USP monograph [4, 5] using a mobile phase of acetonitrile: KH_2PO_4 phosphate buffer (80:20, v/v), at a flow rate of 1.5 mL/min, injection volume of 25 μl , and column oven was maintained at 45°C .

Encapsulation efficiency (EE%) was determined using an ultra-centrifugal filtration (Amicon® Ultra-15, 10 kDa MWCO). EE% was calculated from the azithromycin (AZT) concentration in the filtrate relative to the initial AZT concentration.

In-vitro drug release:

The experiment was carried out using the dialysis bag (molecular-weight cutoff 14 kDa; Membrane Cel MC18 \times 100 CLR, Chicago, IL, USA). The temperature ($37 \pm 0.5^\circ\text{C}$) with and shaking (100 rpm) conditions were maintained by an incubator (Bio-shaker BR-3300LF, Japan). An exact 2 mL of NP sample was transferred in a dialysis bag, which was then immersed in a centrifuge Falcon tube (filled with 25 mL phosphate-buffered saline, PBS pH 7.4). At particular timepoint (1, 2, 4, 6, 8, 10, and 24 h), a

volume of 5mL medium was withdrawn for HPLC quantification and replaced by an equal volume of fresh PBS (n = 3).

Characterizing particle morphology by scanning electron microscopy (SEM)

Nanosuspensions were frozen (-70°C for 12 h) and then lyophilized for 24 h (-50°C , less than 0.1 bar, Alpha 12LD Plus, Christ, Sigma). SEM analysis was carried out with an EVO 25LS scanning electron microscope (Carl Zeiss Microscopy GmbH, Oberkochen, Germany). SEM micrographs were recorded at a magnification of 250 \times with an acceleration voltage of 25 kV under extended vacuum pressure mode. This experiment was performed on representative samples, which were selected based on DLS technique. The experiment was intended to characterize sample morphology before and after CS-addition. Therefore, no statistical evaluation was applied.

Characterizing chemical interactions in nanoparticle structures (via FTIR):

Fourier transform infrared (FTIR) spectroscopy: Before measuring, nanosuspensions were lyophilized (-50°C , less than 0.1 bar, Alpha 12LD Plus, Christ, Sigma). Dry samples were grinded and mixed with potassium bromide (10:1 w/w), then the mixture was compressed into thin layers. FTIR was conducted in the range of 500-4000 cm^{-1} (FT-IR 6700, Jasco, Kyoto, Japan). The FTIR data was recorded on representative samples, which were selected based on DLS technique. The experiment was intended to characterize chemical interaction of samples before and after CS-addition. Therefore, no statistical evaluation was applied.

Determining antibacterial effects via MIC and MBC

The minimum inhibitory concentration (MIC) and minimum bactericidal

concentration (MBC) of free azithromycin (AZT), AZT-PLGA nanoparticles, and AZT-PLGA-CS nanoparticles were determined against *Staphylococcus aureus* using the broth microdilution method, following CLSI guidelines [6, 7]. The bacterial strain *Staphylococcus aureus* ATCC 25923 was kindly provided by the FACM laboratory Laboratory, Université Catholique de Louvain (Bruxelles, Belgium); the sample is stored at -80°C in the Hanoi University of Pharmacy. The nanoparticle concentrations used for MIC/MBC determination were standardized according to the actual AZT content in the formulations.

Briefly, formulations were serially two-fold diluted in Mueller-Hinton Broth (MHB), and 100 μL of each dilution was dispensed into 96-well plates. Bacterial suspensions were prepared from overnight cultures and adjusted to 0.5 McFarland standard, then diluted 1:100 in MHB to obtain a final inoculum of $\sim 1.5 \times 10^6$ CFU/mL. A total of 100 μL of the bacterial suspension was added to each well. Negative control wells contained only MHB without bacteria. Growth control contained MHB with bacteria. Placebo nano-formulations were also prepared and tested [6, 8].

Plates were incubated at 37°C for 20 h. MIC was defined as the lowest concentration with no visible bacterial growth. For MBC determination, all wells with concentrations higher than the MIC were plated onto tryptic soy agar (TSA) and incubated at 37°C for 24, 48, and 72 h, followed by colony counting to determine the lowest. The obtained data was used to calculate Maximal relative efficacy (E_{max}) and Static concentration (C_{static}). In which, C_{static} is the minimum drug concentration required to inhibit net bacterial growth, determined from the concentration-

effect curve. E_{max} expressed as the maximal change in bacterial count ($\log_{10}\text{CFU/mL}$) from the baseline after treatment [6].

Statistical analysis:

The particle size (Z), PDI, and Zeta potentials (ZP) were reported as mean and SD, and ANOVA studies (one-way or two way) were calculated by Graphpad Prism software (7.1, Boston, MA, US). FT-IR results were drawn by Origin Pro (8.1, Northampton, MA, USA).

RESULTS AND DISCUSSIONS

RESULTS

Preparation of AZT -PLGA NPs:

To prepare AZT- PLGA NPs, a screening experiment was carried out by varying the aqueous pH buffers, and drug-to-polymer weight ratios. The drug concentration was maintained at 30 mg per 10 mL solution.

Experiment was conducted with water or phosphate buffer solutions (pH 6.0, 7.4, and 9.0) as the external aqueous phase (Fig. 1A). The results demonstrate a clear pH-dependent variation in particle size. The use of distilled water resulted in particles with an average size of 250 nm, while the formulation prepared in pH 6.0 buffer exhibited the largest size (320 nm). As the pH values increased (7.4 and 9.0), the particle size progressively decreased to approximately 170 nm and 150 nm, respectively. This trend may be attributed to carboxylic groups of PLGA, in which PLGA particles were precipitated at a larger size at acidic media than neutral ones. Meanwhile, PDI values remained below 0.3 for all formulations, indicating acceptable homogeneity. However, using alkaline pH buffer (pH 9.0) might partially hydrolyze or destabilize PLGA matrix. Therefore, pH 7.4 was selected for further investigations.

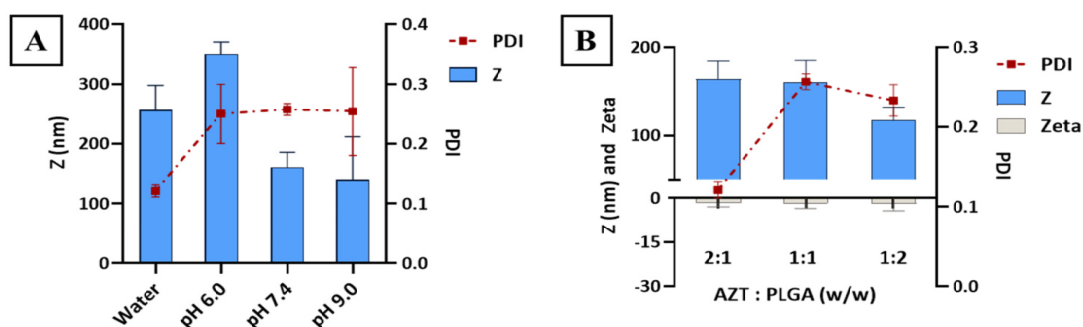


Figure 1: (A) Effect of aqueous phase pH (water, pH 6.0, 7.4, and 9.0 phosphate buffers) and (B) Effect of AZT: PLGA weight ratio (2:1, 1:1, and 1:2) on Z (nm, blue bars, left Y-axis), PDI (red line, right Y-axis), and ZP values (grey bar, left Y-axis).

Fig. 1B presents the impact of AZT: PLGA (w/w) ratios on key physicochemical parameters of NPs. All formulations exhibited low PDI (< 0.3), indicating narrow particle size distribution. An inverse correlation was observed between PLGA content and Z values: Increasing the PLGA proportion (1:2) reduced particle size to below 130 nm. This trend is attributed to improved stabilization and matrix formation with higher polymer content, leading to more compact nanoparticles. Regarding ZP values, the surface charge of all formulations was negative (from 0 to -10 mV). That was due to the presence of carboxylic acid groups on the PLGA surface. Despite low absolute ZP values (negative charges), there was no visible aggregation occurred during 7-day storage. The presence of soluble components (buffer ions and PVA) surrounding the NPs reduced absolute ZP values, but simultaneously provided steric stabilization that helped maintain colloidal stability.

Preparing CS-AZT-PLGA NPs

Chitosan (CS) is an interesting material for nanoparticle-drug delivery due to its biocompatibility, biodegradability, and permeability enhancement. The influence of CS coating on the physicochemical properties

of AZT–PLGA NPs was evaluated at three different AZT:PLGA ratios (2:1, 1:1, and 1:2, Fig. 2A-C, respectively).

For all 3 different formulations of AZT-PLGA NPs, adding CS increased Z values. At a PLGA: CS ratio of 1: 2 (corresponding to the highest CS input), the particle size increased from approximately 157 nm to over 220 nm. This size enlargement can be attributed to the physical layering of CS. Polydispersity index (PDI) values also showed a increasing trend with higher CS levels, indicating broader particle size distributions at higher coating concentrations. Zeta potential (ZP) measurements revealed a clear shift from negative to positive surface charge following CS coating. Compared to uncoated PLGA nanoparticles, CS addition modified ZP gradually. The positive ZP values confirmed successful electrostatic adsorption of the cationic chitosan onto the anionic PLGA nanoparticles and neutralization of surface charge.

As NPs were not isolated from the obtained suspensions, data about Z, PDI, and Zeta were shown to illustrate effects of formulations on these critical quality attributes. Also, in DLS measurement, samples were adequately diluted in water to

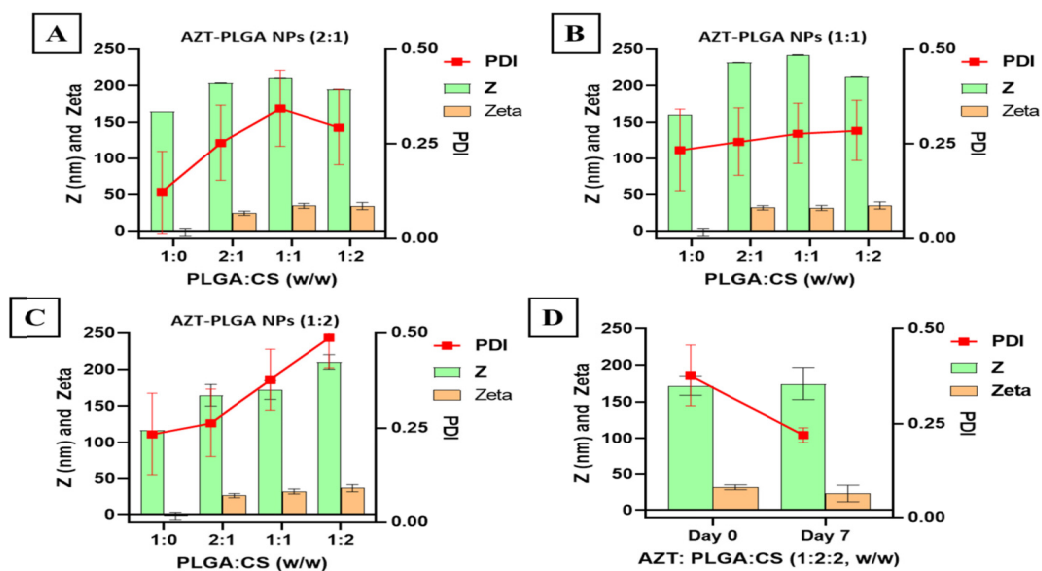


Figure 2: Effect of chitosan (CS) coating at varying PLGA:CS weight ratios (1:0 to 1:2) on three AZT-PLGA NPs formulations.

Table 1: Effects of formulation factors on properties of CS- AZT-PLGA NPs

AZT: PLGA	PLGA: CS	Z (nm)	PDI	ZP	Discussion
2:1	1:0	164.8	Low	-	Acceptable Z and PDI, a low polymer content. CS effects on Z values were insignificant.
	1:2	195.0	High	++	
1:1	1:0	160.5	Low	-	Balanced drug-to-polymer ratio; largest Z values (> 200 nm) might interfere with NPs uptake into bacteria.
	1:1	242.2	Mod.	++	
1:2	1:0	117.3	Low	-	Lower Z and PDI values, a well stable trend of CS effect on Z values.
	1:1	172.3	Mod.	+	
	1:2	210.1	High	++	

Note: For Z (nm), “+”: 100-150 nm, “++”: 150-200 nm, “+++”: more than 200 nm. For ZP (mV): “-”: negative, “+”: 0-30 mV, “++”: more than 30 mV. For PDI: Low: less than 0.2, “Mod...”: moderate, between 0.2-0.3, “High”: more than 0.3.

reduce background scattering and viscosity effects; consequently, water-soluble components like residual PVA or CS at low concentrations had minimal impact on the measured Z values. The observed reversal of zeta potential from negative in PLGA NPs to positive in CS-coated PLGA NPs confirms

successful surface interaction between chitosan and PLGA nanoparticles.

These findings collectively confirm the formation of a CS shell around PLGA nanoparticles, with increasing CS concentration leading to larger, more positively charged particles and broader size

distribution. Based on the evaluation of particle size, polydispersity index (PDI), and zeta potential across various AZT: PLGA and PLGA:CS ratios, Table 1 was prepared.

Among the various formulations investigated, the nanoparticle system composed of AZT and PLGA at a ratio of 1:2 (w/w), coated with CS at a PLGA: CS ratio of 1:1 (w/w), was identified as the optimal formulation. This system exhibited a suitable particle size (less than 200 nm), acceptable size distribution (PDI < 0.3), and the positive ZP value identifying for CS surface coating. These attributes suggest adequate colloidal stability, and potential for improved interaction with biological membranes. As shown in Figure 2D, the Z (nm) and ZP (mV) values of this optimized formulation remained relatively stable over 7 days (storing at 2-8°C). This stability indicates minimal aggregation or degradation within the dispersion medium. In the frame of this study, the AZT-PLGA-CS formulation was suitable to conduct experiments to compare

antibacterial effects of CS-coated NPs and uncoated NPs.

Particle morphology by SEM

The surface morphology and topographic characteristics of AZT-PLGA NPs before and after CS coating were observed using scanning electron microscopy (SEM) and 3D surface mapping derived from SEM micrographs via ImageJ analysis (Fig. 3A-D).

SEM images revealed differences in surface morphology between the two formulations. Uncoated AZT-PLGA NPs (Fig. 5A, top left) showed nearly spherical shapes, the surface of each NP exhibited a relatively smooth and white surface. Although the particle aggregation might be due to the drying and water evaporation process, it can be seen that each particle was separated from each other. In contrast, CS-AZT-PLGA NPs (Fig. 5B, top right) exhibited a more continuous surface texture, with reduced visibility of individual particle boundaries. This morphological transformation suggests the role of a CS

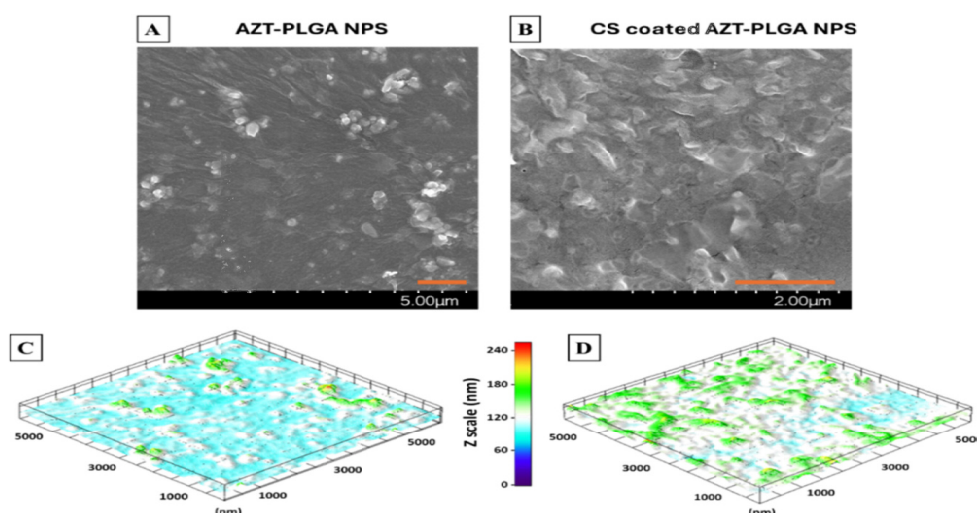


Figure 3: Top: SEM images of (left) AZT-PLGA NPs and (right) CS- AZT-PLGA NPs. Bottom: Corresponding 3D surface topography maps generated from SEM grayscale images using ImageJ. Color gradient reflects surface height distribution (nm), with warmer colors indicating higher features. A-B: orange scale bar of 1000 nm.

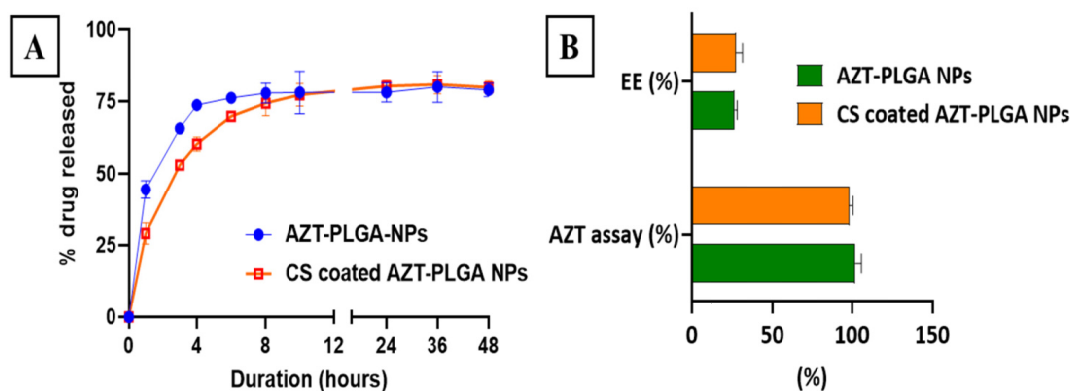


Fig. 4: (A) In vitro release profiles of AZT from uncoated and CS-coated PLGA nanoparticles over 10 hours. (B) Comparison of encapsulation efficiency (EE%) and AZT assay (%) between the two nanoparticle systems. Data expressed as mean \pm SD (n = 3).

layer: As the surface of NPs was covered by CS, it can be said that CS layers were not only covering NPs but also partially formed a matrix among NPs.

To further characterize surface roughness and uniformity, pseudo-3D surface plots were generated from grayscale SEM images using ImageJ (Fig. 5C, bottom). The uncoated NPs demonstrated moderate surface variation, with localized elevations indicated by green-yellow peaks scattering across a relatively flat (blue) background. Conversely, the CS-coated formulation displayed a more homogeneous elevation platform with fewer sharp protrusions, implying a smoother surface layer consistent with polymeric coating. The observed reduction in topographic heterogeneity (lower Z-scale) supports the hypothesis of CS adsorption forming a cohesive outer layer. These findings align with zeta potential data showing surface charge reversal, as well as size increase upon coating, and confirm the structural transformation imparted by CS deposition.

AZT assay and in-vitro drug release study

The results of *in vitro* releases of AZT from uncoated and CS-coated PLGA NPs are

presented in Fig. 4A. The drug content and EE values were presented in Fig. 4B. Both formulations exhibited biphasic release kinetics, consisting of an initial burst phase (in the first duration 3 hours) followed by a sustained release period (from 3 to 10 hours). However, clear differences in release rates and extent were observed between the two systems. For the uncoated AZT-PLGA nanoparticles, the initial burst release reached $44.56 \pm 3.07\%$ at 1 hour, increasing to $65.83 \pm 1.94\%$ at 3 hours. After 10 hours, % AZT released from AZT-PLGA NPs was $78.31 \pm 7.42\%$. This rapid release implies that a significant amount of AZT was localized on the surface of NPs. Also, the porous nature of the PLGA matrix facilitates water penetration and drug diffusion.

Besides, CS-AZT-PLGA NPs demonstrated a slower release rate. At 1 hour, only $29.17 \pm 3.72\%$ of AZT was released, followed by $53.14 \pm 1.09\%$ at 3 hours, these results were significantly lower than those of uncoated NPs. The reduction in early-phase release suggests that the CS coating formed a diffusional barrier on the nanoparticle surface, limiting initial drug efflux and

modulating the overall release profile. Despite slower early-phase release, the total cumulative release after 10 hours was $77.43 \pm 3.91\%$, which is similar to that of uncoated NPs ($p < 0.05$). This indicates that the CS layer primarily delays, rather than reduces, drug diffusion-offering a sustained release advantage without compromising final drug availability. Although the initial burst release may partly result from the dissolution of unencapsulated AZT, this experiment was primarily designed to compare the influence of the chitosan coating on drug release behavior, which clearly demonstrated that CS reduced the early release phase and promoted a more controlled release profile.

Fig. 4B presents that both formulations demonstrated high AZT content ($>98\%$), indicating good formulation integrity. As mentioned, AZT was relatively unstable in acidic pH condition, thereby, carboxylic acid of PLGA might affected the AZT stability. These results confirmed that the preparation process did not impact the AZT concentrations. Besides, % EE of CS coated AZT-PLGA nanoparticles (27.29%) was slightly higher than that of uncoated particles (26.04%). These results suggest that while chitosan coating provides a controlled release advantage, and it also increased EE, which should be considered in formulation optimization.

The *in-vitro* release data of AZT from both NP formulations were fitted to four kinetic models: zero-order, first-order, Higuchi, and Korsmeyer–Peppas (Table 2). The kinetic analysis was performed using data within the first 12 hours, because after this period, the sampling intervals became much longer than those in the early phase (every 2 hours), which could reduce the accuracy of model fitting.

Table 2: In-vitro release data analysis: correlation coefficients (R^2) and Akaike Information Criterion (AIC) values

FORMULATIONS	MODELS	R^2	AIC	n	k
AZI-PLGA	Zero-order	0.58	28.10		
	First-order	0.61	-15.59		
	Higuchi	0.73	25.45		
	Korsmeyer–Peppas (<80 %)	0.85	-27.170	0.236	0.48
AZI-PLGA-CS	Zero-order	0.86	25.97		
	First-order	0.95	-25.08		
	Higuchi	0.95	19.83		
	Korsmeyer–Peppas (<80 %)	0.97	-30.020	0.430	0.31

Among the tested models, the release profiles of both formulations best followed the Korsmeyer–Peppas model ($R^2 > 0.85$ and the lowest AICs). The release exponent (n) of 0.236 for AZT–PLGA, that indicates diffusion-controlled release (Fickian-type), but with a faster, less uniform process, consistent with the initial burst phase you observed. As (n) of 0.430 for AZT-PLGA-CS NPs, that indicates a change toward an anomalous (non-Fickian) transport, in which both diffusion and polymer relaxation contribute to sustained release [9]. In fact, the CS-coated nanoparticles exhibited slightly higher correlation and lower AIC values than the uncoated formulation, suggesting that the CS layer provided an additional diffusional barrier, resulting in a more controlled and sustained release behavior.

Characterizing chemical interactions in nanoparticle structures (via FTIR):

FTIR analysis was employed to elucidate the possible physicochemical interactions among AZT, PLGA, and CS within the nanoparticle formulations. The spectrum of pure AZT exhibited characteristic absorption peaks at 3498 cm^{-1} (O-H and N-H stretching), 2973 and 2936 cm^{-1} (C-H

stretching of aliphatic groups), 1722 cm^{-1} (ester C=O stretching), 1638 cm^{-1} (amide C=O or C=C stretching), and a strong fingerprint region at $1250\text{-}1000\text{ cm}^{-1}$ corresponding to C-O-C and C-N stretching. PLGA displayed prominent peaks at 1750 cm^{-1} (ester carbonyl stretching), $2950\text{-}2970\text{ cm}^{-1}$ (C-H stretching), and $1180\text{-}1080\text{ cm}^{-1}$ (C-O stretching of the ester linkages). The FTIR spectrum of CS showed a broad absorption band around 3400 cm^{-1} due to O-H and N-H stretching, a band near 1590 cm^{-1} attributed to NH_2 bending, and C-O-C stretching around 1000 cm^{-1} .

In the AZT-PLGA NPs spectrum (green line), a shift and broadening of the carbonyl peak and fingerprint region (Fig. 5B, $1250\text{-}1000\text{ cm}^{-1}$) were observed, suggesting hydrogen bonding and hydrophobic interactions between AZT and the PLGA matrix. Notably, in Fig. 5B, alterations in the fingerprint region ($1500\text{-}1000\text{ cm}^{-1}$) confirm molecular interactions and possible changes in the microenvironment of functional groups, indicating successful incorporation of AZT into the PLGA matrix. Additionally, a shift and modifications in the shape and intensity of O-H and N-H stretching (3500

cm^{-1}) of AZT to a larger band with higher peak intensity (green line, Fig. 5C) were detected, that suggests hydrogen bonding between the carbonyl groups of PLGA and hydroxyl or amine groups of AZT.

Upon coating with CS, further spectral changes were evident. The broad O-H/N-H stretching band became more intense and slightly shifted, while additional broadening occurred in the $1000\text{-}1200\text{ cm}^{-1}$ region. These changes suggest strong electrostatic interactions between the protonated amine groups ($-\text{NH}_3^+$) of CS and the terminal carboxylate groups ($-\text{COO}^-$) of PLGA, as well as secondary hydrogen bonding interactions at the nanoparticle surface. The successful deposition of CS onto the nanoparticle surface was thus confirmed by the presence of characteristic chitosan bands superimposed on the AZT-PLGA spectrum. In the AZT-PLGA NP spectrum (green trace), several distinct AZT peaks in the fingerprint region - particularly those around $1050\text{-}1150\text{ cm}^{-1}$, corresponding to C-O stretching and C-N vibrations - appear dampened, broadened, or partially overlapped due to interaction with the PLGA matrix. This is a common phenomenon when drug molecules are

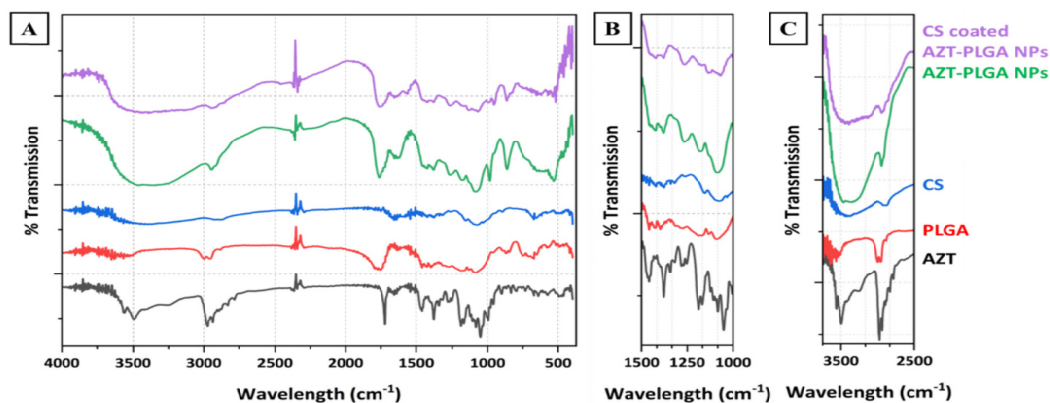


Fig. 5: FTIR spectra of pure components (AZT, PLGA, CS) and the resulting-PLGA NPs and CS-AZT-PLGA NPs, with full-range spectra in panel A, and detailed spectral regions in B and C.

Table 3: Summary of antibacterial effects of AZT-PLGA and CS-AZT-PLGA NPs

NPs formulations with AZT: PLGA:CS (w/w/w ratios)			MIC (mg/L)			MBC (mg/L)			Cstatic	Emax
			24h	48h	72h	24h	48h	72h		
F1	AZT-PLGA	2:1:0	0.25	0.25	0.5	> 4	0.5	0.5	0.169	-3.457
F2	AZT-PLGA	1:2:0	0.25	0.25	0.5	> 4	1	1	0.188	-2.441
F2-1	CS-AZT-PLGA	1:2:1	0.5	0.5	1	> 4	2	2	0.431	-3.204
F2-2	CS-AZT-PLGA	1:2:2	0.25	0.25	0.5	> 4	1	1	0.171	-3.153
AZT	Raw AZT		1	1	1	> 4	2	2	0.429	-2.523

* Note: “X”: MBC was not detected; “Cstatic”: Static concentration, “Emax: maximal relative efficacies.

molecularly dispersed or embedded within a polymer matrix, as seen in encapsulated systems.

Fig. 5C further highlights the broadening and reduced intensity of the O-H/N-H stretching bands around 3450-3300 cm⁻¹ in the AZT-PLGA NPs compared to free AZT and PLGA. This supports the formation of hydrogen bonds and possible disruption of intramolecular hydrogen bonding in AZT upon entrapment, contributing to drug encapsulation stability.

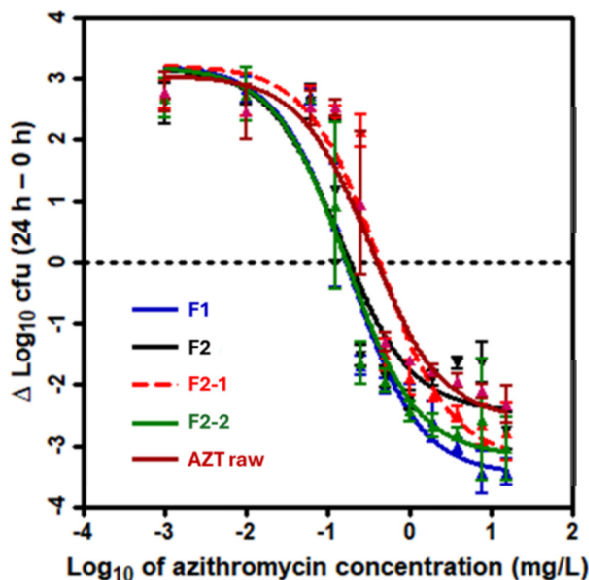
These findings confirm the formation of structurally distinct AZT-PLGA and CS-coated AZT-PLGA nanoparticles and highlight the key molecular interactions responsible for drug entrapment and surface modification.

Antibacterial effects against *Staphylococcus aureus*

The antibacterial efficacy of different AZT-PLGA NPs and CS -AZT-PLGA NPs were evaluated using MIC/MBC testing and time-kill kinetics. As shown in Fig. 6, all formulations demonstrated dose-dependent bacterial killing activity.

In Table 3, raw AZT required a higher concentration (1 mg/L) to achieve MIC and 2 mg/L for MBC, confirming that

Fig. 6: Dose dependent effect of raw AZT, PLGA NPs, CS-PLGA Nps



encapsulation into nanoparticles enhanced antibacterial potency. At 24 h, all nano formulations demonstrated MIC values significantly lower than that of raw AZT prepared in EtOH (1 mg/L). Specifically, F1 (AZT : PLGA 2:1), F2 (AZT: PLGA 1:2), and F2-2 (PLGA:CS 1:1) showed MICs of 0.25 mg/L-four times lower than the raw drug-while F2-1 (PLGA:CS 2:1) exhibited an MIC of 0.5 mg/L, still two-fold lower than raw AZT. The placebo formulations (PLGA

and CS-PLGA NPs) showed no bactericidal effects (there was no MIC detected). Time-kill curves (Fig. 6) further corroborated these findings. F1, F2, F2-2 induced a more rapid and pronounced bacterial reduction within 24 h at higher concentrations compared to F2-1 and raw AZT (Fig. 6).

AZT is a bacteriostatic agent, and as expected, no minimum bactericidal concentration (MBC) was detected for any formulation at the 24 h timepoint. However, upon extending the exposure to 48 h and 72 h, MBC values were observed for all nanoparticle systems. Based on Emax values (Table 2), all the samples (both NPs and raw drug) displayed values in the range from -2.5 to -3 Log₁₀CFU, that implies that the main effect was based on AZT effect. However, the difference in MIC and C_{static} among F1, F2, F2-2 (compared to raw AZT) showed that PLGA NPs and CS-PLGA NPs significantly improved antibacterial effect due to their formulation effects of PLGA and CS [6, 10, 11]: NPs formulation improved drug solubility, sustained release kinetics, and increased interaction with bacterial membranes.

The rapid onset of action and lower MICs observed in F1 may result from higher AZT content relative to PLGA, in which the instable NPs structure facilitated faster drug availability. The F2-1 formulation (PLGA:CS 2:1) showed reduced activity, likely due to incomplete or inconsistent chitosan coating, as previously noted in physicochemical characterizations. In contrast, F2-2 (PLGA:CS 1:1) achieved a more uniform surface modification, possibly aiding in controlled release while preserving antibacterial performance.

Overall, the results suggest that nanoparticle-based delivery systems can

enhance AZT efficacy, and that optimal CS-coating must balance structural stability and drug release. Among tested formulations, F2-2 is considered the most promising candidate, combining improved physicochemical characteristics with sustained antibacterial action.

DISCUSSION

Throughout the emulsification–solvent evaporation process, AZT-PLGA NPs were prepared at nanoscale particles with narrow dispersity, which are similar to previous publications [1, 3, 4]. Previously, AZT : PLGA ratios ranging from 1:1 to 1:3 were explored [3, 4]; however, this paper presents different aqueous phases as well as a greater range of AZT: PLGA w/w ratios. Importantly, the preparation of CS-coated AZT–PLGA NPs and effects of CS on AZT-PLGA NPs has not been explored before. Here, our study is the first to investigate and characterize CS-coated AZT–PLGA NPs against *S. aureus*, including MIC, MBC, and time-kill kinetics, offering new insights into surface-modified polymeric nanocarriers for improved antibacterial performance. The kinetic analysis (Table 2) confirmed that the release of AZT from PLGA and CS-coated PLGA nanoparticles was governed by a combination of diffusion and polymer degradation. In the diffusion-controlled stage, AZT molecules migrated through hydrophilic pores of the dialysis membrane and through microchannels within the PLGA matrix (Fickian mechanism). Subsequently, as the PLGA and CS matrices swelled and gradually degraded, additional AZT was released by erosion of the CS-PLGA polymer network. This interpretation is consistent with the FTIR results and the relatively low encapsulation efficiency (EE%), which together support the presence of both

encapsulated and surface-associated drug fractions.

The results clearly demonstrate that encapsulating azithromycin (AZT) within PLGA nanoparticles significantly enhances its antibacterial activity against *Staphylococcus aureus* compared to the raw drug. The optimized AZT-PLGA NPs (F2) exhibited lower MIC and MBC values, particularly after 48–72 h, which can be attributed to sustained drug release and improved nanoparticle–bacteria interactions. The addition of a chitosan (CS) coating (F2-2) further modified the surface properties, shifting the zeta potential from negative to positive and introducing a bio-adhesive, cationic surface. While MIC/MBC values of F2 and F2-2 were comparable, calculated E_{max} and static concentration showed that F2-2 (CS-coated AZT-PLGA NPs) exhibited a better effect than AZT-PLGA NPs. CS coating likely facilitated enhanced bacterial surface binding and prolonged drug–bacteria contact time, thus improving bactericidal efficiency in extended exposure [2]. These findings support the use of biodegradable, surface-functionalized nanoparticles as an effective platform for improving the delivery and therapeutic outcomes of macrolide antibiotics such as AZT.

Compared to study of Mohadi et al. (2014) [3], where AZT-PLGA NPs demonstrated an enhancement in activity against *Salmonella typhi*, our AZT-PLGA NPs showed a consistent 4-fold improvement over raw AZT against *S. aureus*. This difference may arise from the intrinsic susceptibility differences between Gram-negative *S. typhi* and Gram-positive *S. aureus*. In relation to study of Kerdmanee et al. [12], who developed hydrogel-based AZT niosomes (AZG) for periodontal pathogens, our system shows

greater specificity in quantitative MIC/MBC assessment rather than zone-of-inhibition diameters. Although both studies confirmed the superiority of nanoformulations over free AZT, our PLGA-based NPs showed measurable and time-dependent bactericidal activity, particularly in MBC values at 48–72 h, which was not observed in their hydrogel system. When comparing with study of Yasmin Abo-zeid et al. [1], their study reported MICs of 64 $\mu\text{g/mL}$ for AZT-PLGA NPs (F5 and F10), targeting *MRSA* and *E. faecalis*, which are known to be more resistant than *S. aureus*. Therefore, it is a suggestion for this study to test effects of CS coated AZT-PLGA NPs on resistant bacteria in the near future. Although several studies have reported the intrinsic antibacterial activity of CS [13], this effect strongly depends on its protonated state at acidic pH [2, 13, 14]. In the present study, the nanoparticles were dispersed in PBS at pH 7.4, where the amino groups of CS are largely deprotonated; therefore, neither PLGA nor CS is expected to exhibit direct antibacterial activity under these conditions.

The nanoparticles were not isolated after solvent-evaporation, in which physicochemical and microbiological characterizations were conducted on the obtained samples. Here, obtained results offered information about the trends of formulation impacts (related to CS) on physicochemical interactions, and antibacterial properties of the nano-systems. Furthermore, in DLS measurement, samples were adequately diluted in water to reduce background scattering and viscosity effects; consequently, water-soluble components like residual PVA or CS at low concentrations had minimal impact on the measured Z values. The observed reversal of zeta potential from

negative in PLGA NPs to positive in CS-coated PLGA NPs confirms successful surface interaction between chitosan and PLGA nanoparticles.

CONCLUSION

In summary, AZT-loaded PLGA NPs (with a particle size of less than 200 nm) significantly improved antibacterial efficacy against *S. aureus* compared to raw AZT. Coating CS onto PLGA NPs surface modified ZP values, enhanced sustained release and

relatively modified bacterial inhibition. The findings support potentiality of NPs for advanced antimicrobial delivery systems.

ACKNOWLEDGMENTS

This study was supported by the university project, Hanoi University of Pharmacy (QĐ 1472-QĐ-DHN).

CONFLICTS OF INTEREST

None.

REFERENCES

1. Abo-Zeid Y, Amer A, Bakkar MR, El-Houssieny B, Sakran W. Antimicrobial Activity of Azithromycin Encapsulated into PLGA NPs: A Potential Strategy to Overcome Efflux Resistance. *Antibiotics (Basel)*. 2022;11(11).
2. Chandrasekaran M, Kim KD, Chun SC. Antibacterial Activity of Chitosan Nanoparticles: A Review. *Processes*. 2020;8(9):1173.
3. Mohammadi G, Valizadeh H, Barzegar-Jalali M, Lotfipour F, Adibkia K, Milani M, et al. Development of azithromycin-PLGA nanoparticles: physicochemical characterization and antibacterial effect against *Salmonella typhi*. *Colloids Surf B Biointerfaces*. 2010;80(1):34-9.
4. Tran BN, Le Ha C, Vu DTT, Nguyen CN. Development and In Vitro Characterization of Azithromycin-PLGA Nanoparticles Loaded Thermoresponsive Hydrogels: A Quality by Design Approach Toward Intra-Articular Delivery of Macrolides. *AAPS PharmSciTech*. 2025;26(6):171.
5. Commission U. USP 41-NF. Azithromycin monograph. FDA2023.
6. Nguyen TK, Peyrusson F, Dodémont M, Pham NH, Nguyen HA, Tulkens PM, et al. The Persister Character of Clinical Isolates of *Staphylococcus aureus* Contributes to Faster Evolution to Resistance and Higher Survival in THP-1 Monocytes: A Study With Moxifloxacin. *Front Microbiol*. 2020;Volume 11 - 2020.
7. Weinstein MP, Limbago B, Patel J, Mathers A, Campeau S, Mazzulli T, et al. M100 performance standards for antimicrobial susceptibility testing. *J Clin Microbiol*. 2018;27:210-4.
8. Nguyen TK, Peyrusson F, Siala W, Pham NH, Nguyen HA, Tulkens PM, et al. Activity of moxifloxacin against biofilms formed by clinical isolates of *Staphylococcus aureus* differing by their resistant or persister character to fluoroquinolones. *Front Microbiol*. 2021;12:785573.
9. Peppas NA, Korsmeyer RW. Dynamically swelling hydrogels in controlled release applications. *Hydrogels in medicine and pharmacy*; 1987 (3). p. 109-136.
10. Fonseca C, Simoes S, Gaspar R. Paclitaxel-loaded PLGA nanoparticles: preparation, physicochemical characterization and in vitro anti-tumoral activity. *J Control Release*. 2002;83(2):273-86.
11. Tran BN, Nguyen HT, Kim JO, Yong CS, Nguyen CN. Developing combination of artesunate with paclitaxel loaded into poly-d,l-lactic-co-glycolic acid nanoparticle for systemic delivery to exhibit synergic chemotherapeutic response. *Drug Dev Ind Pharm*. 2017;43(12):1952-62.
12. Kerdmanee K, Phaechamud T, Limsitthichaiakoon S. Thermoresponsive Azithromycin-Loaded Niosome Gel Based on Poloxamer 407 and Hyaluronic Interactions for Periodontitis Treatment. *Pharmaceutics*. 2022;14(10).
13. Hosseinnejad M, Jafari SM. Evaluation of different factors affecting antimicrobial properties of chitosan. *Int J Biol Macromol*. 2016;85:467-75.
14. Raafat D, Sahl HG. Chitosan and its antimicrobial potential—a critical literature survey. *Microb Biotechnol*. 2009;2(2): 186-201.